SCIENTIFIC REPORTS

OPEN

SUBJECT AREAS:
BATTERIES
RENEWABLE ENERGY

Received
17 November 2014

Accepted
16 January 2015

Published
16 February 2015

Correspondence and requests for materials should be addressed to D.-L.P. (dlpeng@xmu.edu.cn)

Facile fabrication of various zinc-nickel citrate microspheres and their transformation to ZnO-NiO hybrid microspheres with excellent lithium storage properties

Qingshui Xie, Yating Ma, Deqian Zeng, Laisen Wang, Guanghui Yue & Dong-Liang Peng

Fujian Key Laboratory of Advanced Materials, Collaborative Innovation Center of Chemistry for Energy Materials, Department of Materials Science and Engineering, College of Materials, Xiamen University, Xiamen 361005, China.

Zinc-nickel citrate microspheres are prepared by a simple aging process of zinc citrate solid microspheres in nickel nitrate solution. As the concentration of nickel nitrate solution increases, the morphology of the produced zinc-nickel citrate evolves from solid, yolk-shell to hollow microspheres. The formation mechanism of different zinc-nickel citrate microspheres is discussed. After annealing treatment of the corresponding zinc-nickel citrate microspheres in air, three different ZnO-NiO hybrid architectures including solid, yolk-shell and hollow microspheres can be successfully fabricated. When applied as the anode materials for lithium ion batteries, ZnO-NiO hybrid yolk-shell microspheres demonstrate the best electrochemical properties than solid and hollow counterparts. After 200th cycles, ZnO-NiO hybrid yolk-shell microspheres deliver a high reversible capacity of 1176 mA h g^{-1}. The unique yolk-shell configuration, the synergetic effect between ZnO and NiO and the catalytic effect of metal Ni generated by the reduction of NiO during discharging process are responsible for the excellent lithium storage properties of ZnO-NiO hybrid yolk-shell microspheres.

Nowadays, a great deal of efforts have been devoted to explore the advanced electrode materials for replacing the commercially available graphite anodes in lithium ion batteries in order to meet the ever growing requirements in various energy consumption devices, such as electric vehicles and hybrid electric vehicles[1–5]. Transition metal oxides with porous structures have been extensively synthesized recently and when used as the electrode materials they show higher theoretical capacity compared to traditional carbonaceous materials[6–13]. Among them, ZnO as one of the fascinating multifunctional semiconductor can contribute to a high theoretical capacity of 978 mA h g^{-1} both through the conversion and alloying/dealloying reactions and holds bright prospects as the advanced anode material for next-generation lithium ion batteires[14–17]. Unfortunately, the practical application of ZnO in lithium ion batteries has been greatly restricted because of its drastic volume variation (over 228%) during cycling and intrinsic poor electronic conductivity which would cause the severe capacity decay and unsatisfactory cyclability[18]. How to effectively improve the specific capacity and cycling stability of ZnO electrode become one of the urgent tasks that needs to be resolved currently. Previous reports have shown that the rational hollow constructing is an effective strategy to strengthen the lithium storage properties of electrode materials[9,10,19–25]. For instance, Kang's group successfully synthesized yolk-shell NiO microspheres which exhibited significantly enhanced electrochemical properties compared to nano-cubic NiO powders[22]. So, it is of great significance to prepare various ZnO hollow structures which may possess the good lithium storage properties.

On the other hand, mixed metal oxides have been adopted as the anode materials in lithium ion batteries in very recent years in order to strengthen the electrochemical properties through the synergetic effect between the different components[26–29]. For example, double-shelled Fe_2O_3/Co_3O_4 hollow microcubes prepared by Yin's group demonstrated improved lithium storage properties in comparison with single Co_3O_4 nanoparticles[26]. The superior electrochemical properties of hybrid microcubes originate from their special hollow structures, and the

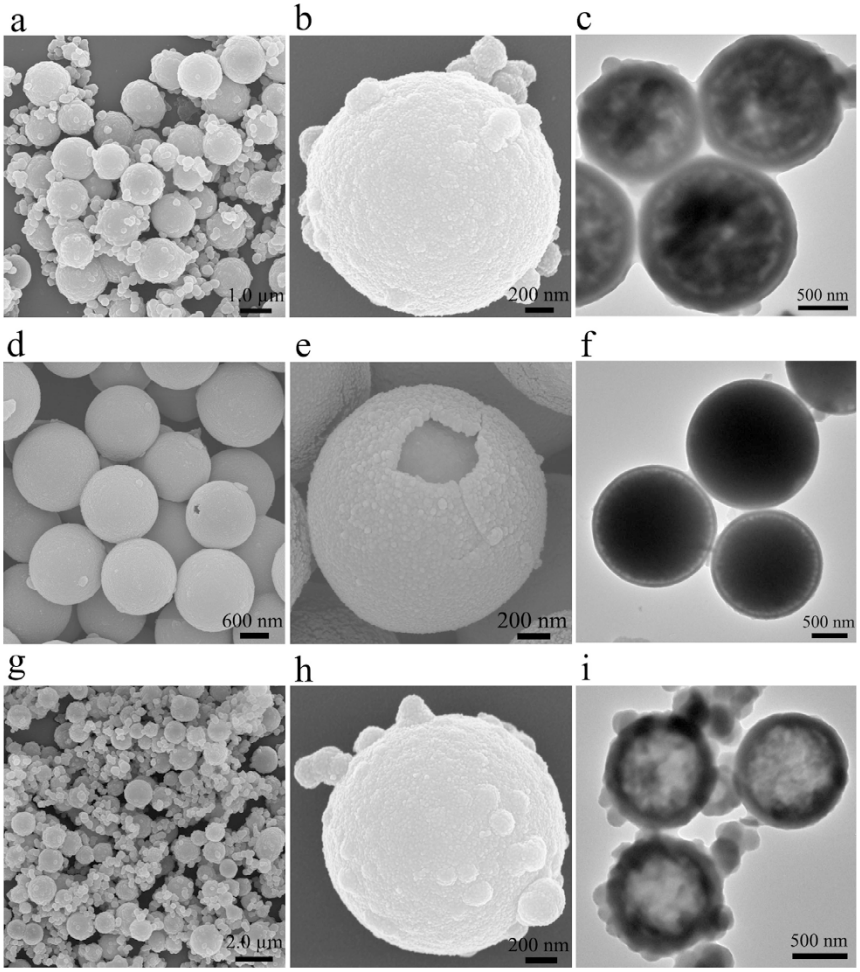

Figure 1 | The SEM and TEM images of zinc-nickel citrate yolk-shell (a–c), solid (d–f) and hollow (g–i) microspheres.

decoration of Fe_2O_3 that possesses the better electronic conductivity than Co_3O_4, giving rise to the decrease of the charge transfer resistance of hybrid electrodes. NiO has been deemed as the promising anode candidate in lithium ion batteries because of its special merits including large theoretical capacity (718 mA h g^{-1}), nontoxicity as well as rich resource in nature[30–32]. Inspired by the above-mentioned design concepts, combining ZnO with NiO to prepare ZnO-NiO hybrid hollow micro/nanostructures towards enhancing the lithium storage properties has become a very meaningful research work. To the best of our knowledge, yolk-shell ZnO-NiO hybrid microspheres used as the anode materials for lithium ion batteries have not been reported so far.

In this work, various zinc-nickel citrate microspheres can be produced by aging the zinc citrate solid microspheres in nickel nitrate solution. The influences of the concentration of nickel nitrate solution and the aging time on the morphology, composition and microstructure of the obtained zinc-nickel citrate are investigated in detail. ZnO-NiO hybrid solid, yolk-shell and hollow microspheres with good morphological inheritance can be fabricated via a heating treatment of the corresponding zinc-nickel citrate microspheres. ZnO-NiO hybrid yolk-shell microspheres manifest the best lithium storage properties than solid and hollow counterparts when utilized as the anode materials for lithium ion batteries. The reasons for the exceptional electrochemical properties of yolk-shell hybrid microspheres are interpreted.

Results

Characterizations of zinc-nickel citrate microspheres. Zinc-nickel citrate harvested after aging in 0.15 M of nickel nitrate solution for 1 h was measured by SEM and TEM to disclose its morphology and microstructure. As exhibited in Fig. 1a, the produced zinc-nickel citrate consists of dispersed microspheres with the average diameter of 1.5 μm. Many nanoparticles, having the particle size of approximate 350 nm, attach on the surface of microspheres, depicting the relatively rough surface (Fig. 1a and 1b). Energy dispersive spectroscopy (EDS) measurement (Supplementary Fig. S1a) implies the presence of Zn, Ni, O and C with a Ni/Zn molar ratio of 0.58. The TEM macrograph shown in Fig. 1c corroborates the yolk-shell structures of the obtained zinc-nickel citrate microspheres aged at 0.15 M of nickel nitrate solution. The distinct bright and dark regions in the center of microspheres indicate that the core material is packed loosely and contains a lot of pores.

The influence of the concentration of nickel nitrate solution on the morphology and microstructure of the collected zinc-nickel citrate was investigated in detail. From Fig. 1d–f, zinc-nickel citrate microspheres with no obvious yolk-shell structures can be prepared when the concentration of nickel nitrate reduces to 0.1 M. Due to the very small void space between the core and the shell, we denote these type of microspheres as solid microspheres in order to distinguish from above clear yolk-shell microspheres obtained from the concentration of 0.15 M. Differently, the surface of zinc-nickel citrate solid microspheres is smoother than that of yolk-shell counterparts. Almost no additional nanoparticles attach on the surfaces of solid microspheres. The Ni/Zn molar ratio of zinc-nickel citrate solid microspheres is about 0.093 (Supplementary Fig. S1b). As the concentration of nickel nitrate solution increases to 0.2 M, zinc-nickel citrate hollow microspheres can be synthesized (Fig. 1g–i). More nanoparticles form on the surfaces of hollow microspheres at this condition. The Ni/Zn

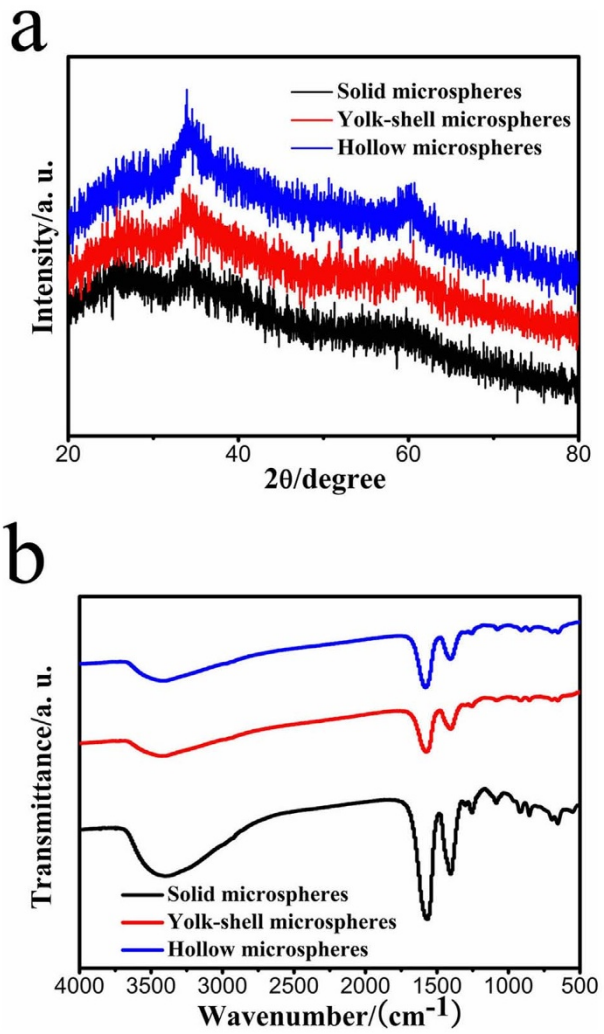

Figure 2 | The XRD patterns (a) and FT-IR spectra (b) of zinc-nickel citrate solid, yolk-shell and hollow microspheres.

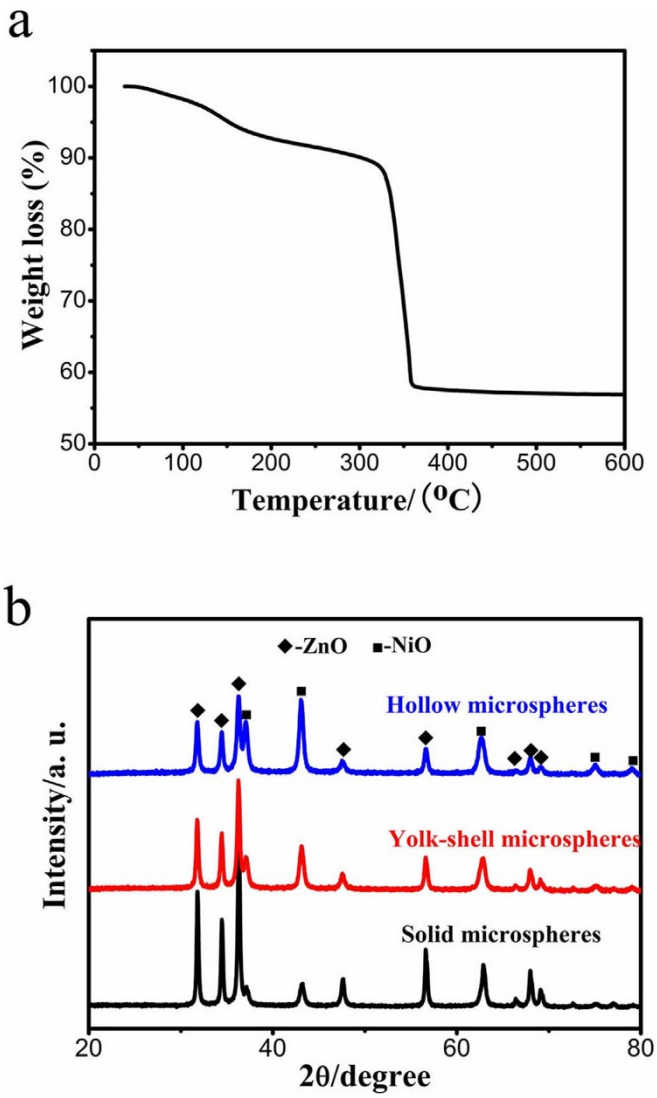

Figure 3 | (a) TGA curve of zinc-nickel citrate yolk-shell microspheres. (b) The XRD patterns of ZnO-NiO solid, yolk-shell and hollow hybrid microspheres.

molar ratio of zinc-nickel citrate hollow microspheres increases to 1.05 (Supplementary Fig. S1c). The diameters of zinc-nickel citrate solid and hollow microspheres do not change obviously compared to above yolk-shell microspheres. Further increasing the concentration of nickel nitrate solution to 0.3 M, only irregular nanoparticles with particle size ranging from 300 to 500 nm can be observed (Supplementary Fig. S2a). The Ni/Zn molar ratio further increases to 1.60 (see also Supplementary Fig. S2b). Differently, the aging time do not have a decisive effect on the morphology and composition of the obtained zinc-nickel citrate (Supplementary Fig. S3 and Fig. S4).

The XRD patterns of the collected zinc-nickel citrate solid, yolk-shell and hollow microspheres are manifested in Fig. 2a, from which one can find that all three samples are mainly amorphous. There are two small diffraction peaks in each zinc-nickel citrate precursor, differentiating from the initial amorphous zinc citrate solid microspheres, which is attributed to the crystallization of small amount of zinc citrate[33]. In our earlier literature, we have demonstrated that the formed zinc citrate nanocrystals during aging process have a size less than 10 nm from HRTEM observation[33]. Moreover, the intensities of these two peaks strengthen gradually from solid, yolk-shell to hollow microspheres, hinting that the dissolution-redeposition process of zinc citrate takes place more intensely as increasing the concentration of nickel nitrate solution during aging process (discussed below) and more zinc citrate crystallize in the amorphous matrix. The FT-IR spectra of all three samples display the similar curves in shape as illustrated in Fig. 2b. The presence of carboxylate acid groups (-COO^-) is evidenced from the strong peaks located at 1574.5 and 1403.3 cm^{-1} [33,34]. The peak centered at 3410 cm^{-1} arises from the -OH groups. All above results suggest that zinc-nickel citrate can be prepared by aging zinc citrate solid microspheres in nickel nitrate solution. The concentration of nickel nitrate solution plays an important role in the morphology and composition of the obtained zinc-nickel citrate. As the concentration of nickel nitrate solution increases from 0.1, 0.15 to 0.2 M, the morphologies of the produced zinc-nickel citrate evolve from solid, yolk-shell to hollow microspheres. The content of Ni in zinc-nickel citrate also increases with the concentration of nickel nitrate solution. The TG evaluation of zinc-nickel citrate yolk-shell microspheres obtained at 0.15 M of nickel nitrate solution for 1 h is exhibited in Fig. 3a. The large weight loss between 310 and 360°C is caused by the transformation of zinc-nickel citrate to ZnO-NiO hybrids. So, 500°C is used as the annealing temperature to completely convert zinc-nickel citrate microspheres into ZnO-NiO hybrids.

Characterizations of ZnO-NiO hybrid microspheres. The XRD patterns of the synthesized ZnO-NiO hybrids through heating treatment of zinc-nickel citrate solid, yolk-shell and hollow microspheres at 500°C for 2 h are demonstrated in Fig. 3b. In each

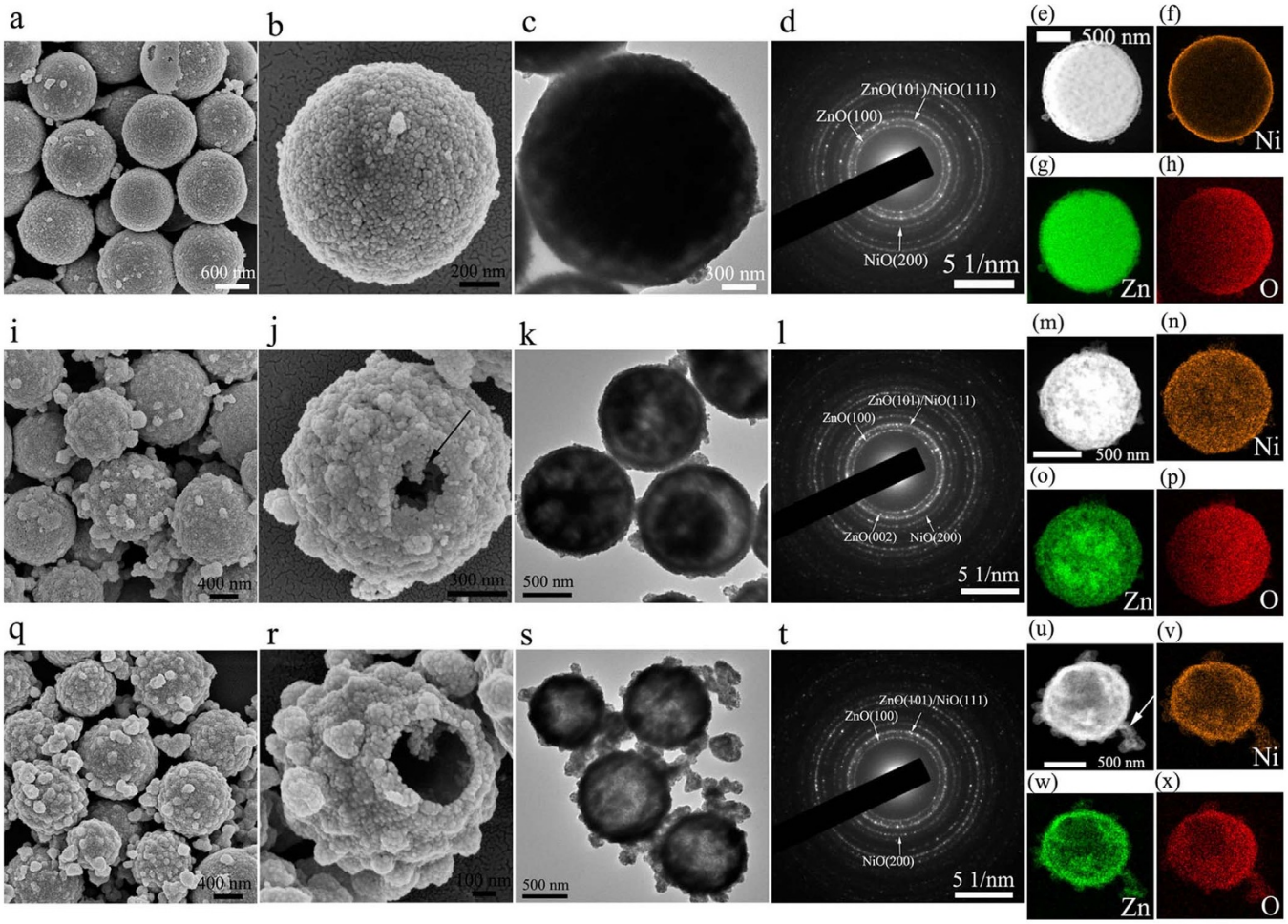

Figure 4 | The SEM (a–b, i–j and q–r), TEM (c, k and s) micrographs and SAED patterns (d, l and t) of ZnO-NiO solid, yolk-shell and hollow hybrid microspheres, respectively. HAADF STEM images (e, m and u) and the elemental mappings of Ni (f, n and v), Zn (g, o and w) and O (h, p and x) of ZnO-NiO solid, yolk-shell and hollow hybrid microspheres, respectively.

hybrid, the diffraction peaks can be attributed to hexagonal ZnO (JCPDS card no. 36-1451) and cubic NiO (JCPDS card no. 65-2901). No impurity peaks can be distinguished, indicating the good purity of the obtained ZnO-NiO hybrids. Additionally, the NiO diffraction peaks strengthen gradually, implying the increasing NiO content from solid, yolk-shell to hollow hybrid microspheres.

ZnO-NiO hybrids fabricated by calcination of zinc-nickel citrate solid, yolk-shell and hollow microspheres in air were evaluated by SEM and TEM. As revealed in Fig. 4, ZnO-NiO hybrid solid, yolk-shell and hollow microspheres can be successfully produced, well inheriting the morphologies of their respective precursors. The particle sizes of the hybrid microspheres range from 1.1 to 1.3 μm. ZnO-NiO hybrid hollow microspheres show the roughest surface, followed by yolk-shell microspheres and solid microspheres. Many nanoparticles with the diameter ranging from 150 to 200 nm attach on the surfaces of ZnO-NiO hybrid hollow and yolk-shell microspheres, while only a few smaller nanoparticles can be seen in ZnO-NiO hybrid solid microspheres. As increasing the concentration of nickel nitrate, more zinc-nickel citrate nanoparticles form on the surfaces of yolk-shell and hollow microspheres due to the enhanced interactions between the carboxylate acid groups and nickel ions during aging process (Fig. 1 and Fig. 5). After heating treatment, zinc-nickel citrate nanoparticles are converted to ZnO-NiO hybrid nanoparticles which attach on the surfaces of hybrid microspheres, leading to rougher surfaces of ZnO-NiO hybrid yolk-shell and hollow microspheres than solid counterparts. The presence of ZnO and NiO in all three hybrids is further testified by the corresponding SAED patterns illustrated in Fig. 4d, 4l and 4t. EDS measurements suggest that the Ni/Zn molar ratios in ZnO-NiO hybrid solid, yolk-shell and hollow microspheres almost do no change after calcination (Supplementary Fig. S5). In order to explore the distribution of Zn, Ni and O elements in all three hybrid microspheres, high-angle annular dark-field (HAADF) scanning TEM (STEM) images and the corresponding element distributions of the solid, yolk-shell and hollow hybrid microspheres are displayed in Fig. 4(e–h), 4(m–p) and 4(u–x), respectively. Ni element mainly distributes on the outer thin shell of ZnO-NiO solid hybrid microspheres, while Zn and O elements have a uniform distribution throughout the whole microsphere. For ZnO-NiO yolk-shell hybrid microspheres, Ni element still mainly distributes on the shell of the microspheres. The Ni signal of the yolk-shell hybrid microspheres is stronger than that of solid hybrid counterparts, indicating the higher content of NiO in the shell of yolk-shell hybrid microspheres. Differently, the Zn signal in the center region is stronger than that in the outer shell region, indicating the higher ZnO content in the core region than the shell region. O element has a homogeneous distribution within the microsphere. From the different element distributions of Zn, Ni and O, it can be rationally deduced that the shells of yolk-shell hybrid microspheres are made up of ZnO and NiO, however, the cores are possibly dominated by ZnO. In the case of ZnO-NiO hollow hybrid microspheres, Ni, Zn and O elements have homogeneous distributions throughout the hollow microsphere as well as in the nanoparticle marked by the white arrow.

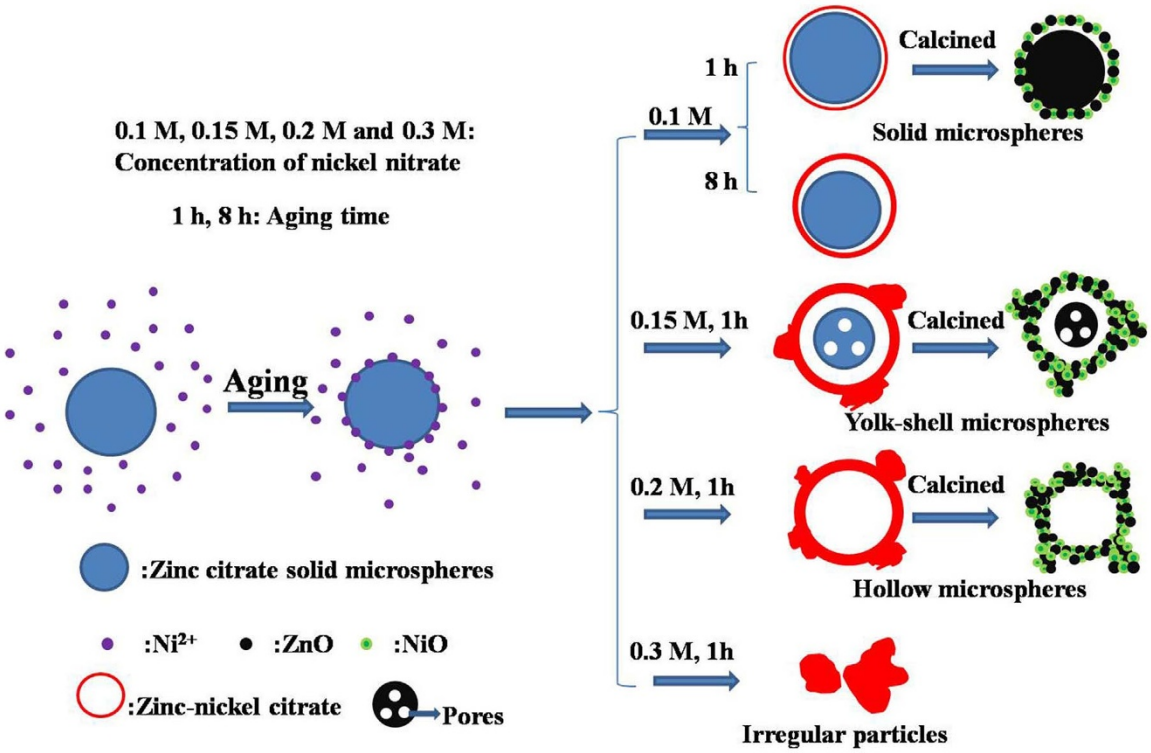

Figure 5 | **A schematic formation process of various zinc-nickel citrate microspheres and ZnO-NiO solid, yolk-shell and hollow hybrid microspheres.**

Discussion

On the basis of above SEM and TEM observations and analysis, a plausible formation process for various ZnO-NiO hybrid microspheres is proposed and illustrated in Fig. 5. By dispersing zinc citrate solid microspheres in nickel nitrate solution, Ni^{2+} would interact with the $-COO^-$ and -OH groups available on the surface of zinc citrate solid microspheres by means of the electrostatic interplays during aging process. Then, a very thin zinc-nickel citrate layer would form on the outermost surface of zinc citrate solid microspheres. Subsequently, this zinc-nickel citrate thin layer would act as the initial redeposition site and a dissolution-redeposition process occurs at a particular region underneath the thin layer. The concentration of nickel nitrate solution exerts significant effect on the morphology and composition of the finally obtained zinc-nickel citrate microspheres. At a low concentration of nickel nitrate solution (0.1 M), this dissolution-redeposition process proceeds no obviously, leading to the formation of zinc-nickel citrate microspheres with no obvious yolk-shell structures (named as solid microspheres above). In this concentration, the small amount of Ni exists on the outermost shell of solid microspheres, evidenced by the Ni element mapping in Fig. 4f. The produced zinc-nickel citrate solid microspheres almost maintain the amorphous characteristic (Fig. 2a) and no additional nanoparticles form. Increasing the aging time to 8 h, no obvious morphology change of zinc-nickel citrate microspheres can be found. As further increasing the concentration of nickel nitrate solution to 0.15 M, the inner zinc citrate core would dissolve into nickel nitrate solution due to its larger curvature compared to the outer shell, interact with nickel ions and then redeposite on the outermost zinc-nickel citrate thin layer of microspheres, giving rise to the formation of zinc-nickel citrate yolk-shell microspheres. This behavior is similar to the formation of zinc citrate yolk-shell microspheres reported in our earlier literature[33]. During this process, the crystallization of a small amount of zinc citrate takes place, resulting in the two small diffraction peaks in the XRD pattern (Fig. 2a). The shell thickness of zinc-nickel citrate yolk-shell microspheres increases at the cost of the consumption of zinc citrate cores. As a result, the core becomes loosely packing and many pores forms. In addition, a small amount of zinc-nickel citrate nanoparticles generate on the surface of yolk-shell microspheres. When the concentration of nickel nitrate solution reaches to 0.2 M, the zinc citrate cores completely dissolve and disappear, leading to the formation of zinc-nickel citrate hollow microspheres. More amount of zinc-nickel citrate nanoparticles generate on the surface of hollow microspheres at this stage. Further increasing the concentration of nickel nitrate solution to 0.3 M, the microspherical structures of zinc-nickel citrate are destroyed, leading to the generation of irregular nanoparticles with large particle size of 300–500 nm. Finally, zinc-nickel citrate solid, yolk-shell and hollow microspheres are employed as the corresponding precursors to successfully fabricate ZnO-NiO solid, yolk-shell and hollow hybrid microspheres through an annealing treatment. ZnO-NiO hollow hybrid microspheres possess the largest surface area (24.1 $m^2 g^{-1}$), followed by yolk-shell (18.7 $m^2 g^{-1}$) and solid counterparts (12.8 $m^2 g^{-1}$) on the basis of N_2 adsorption-desorption measurements shown in Supplementary Fig. S6. The pore sizes in ZnO-NiO solid, yolk-shell and hollow hybrid microspheres are mainly centered at 26.4, 18.3 and 18.9 nm, respectively, indicating the mesoporous structures of all three hybrid microspheres (the insets in Supplementary Fig. S6). The presence of mesopores in electrode materials is conducive to the diffusion of electrolyte within the electrode and can effectively accommodate the volume variation during cycling, resulting in the improvement of lithium storage properties[19,35,36].

The CV tests of all three ZnO-NiO hybrid microspheres are operated at 0.1 mV s^{-1} in 0.01–3 V in order to help us to well understand the electrochemical reaction mechanism during cycling and the corresponding results are displayed in Fig. 6a–c. All three ZnO-NiO hybrids demonstrate the similar curves in shape. In the initial cathodic sweep, an intense and sharp reduction peak at around 0.27 V (where solid microsphere is 0.26 V, yolk-shell microsphere is 0.27 V, hollow microsphere is 0.33 V) can be seen clearly. This peak is caused by a combination of several electrode reactions at close potentials, including the reduction of ZnO and NiO to Zn and Ni along

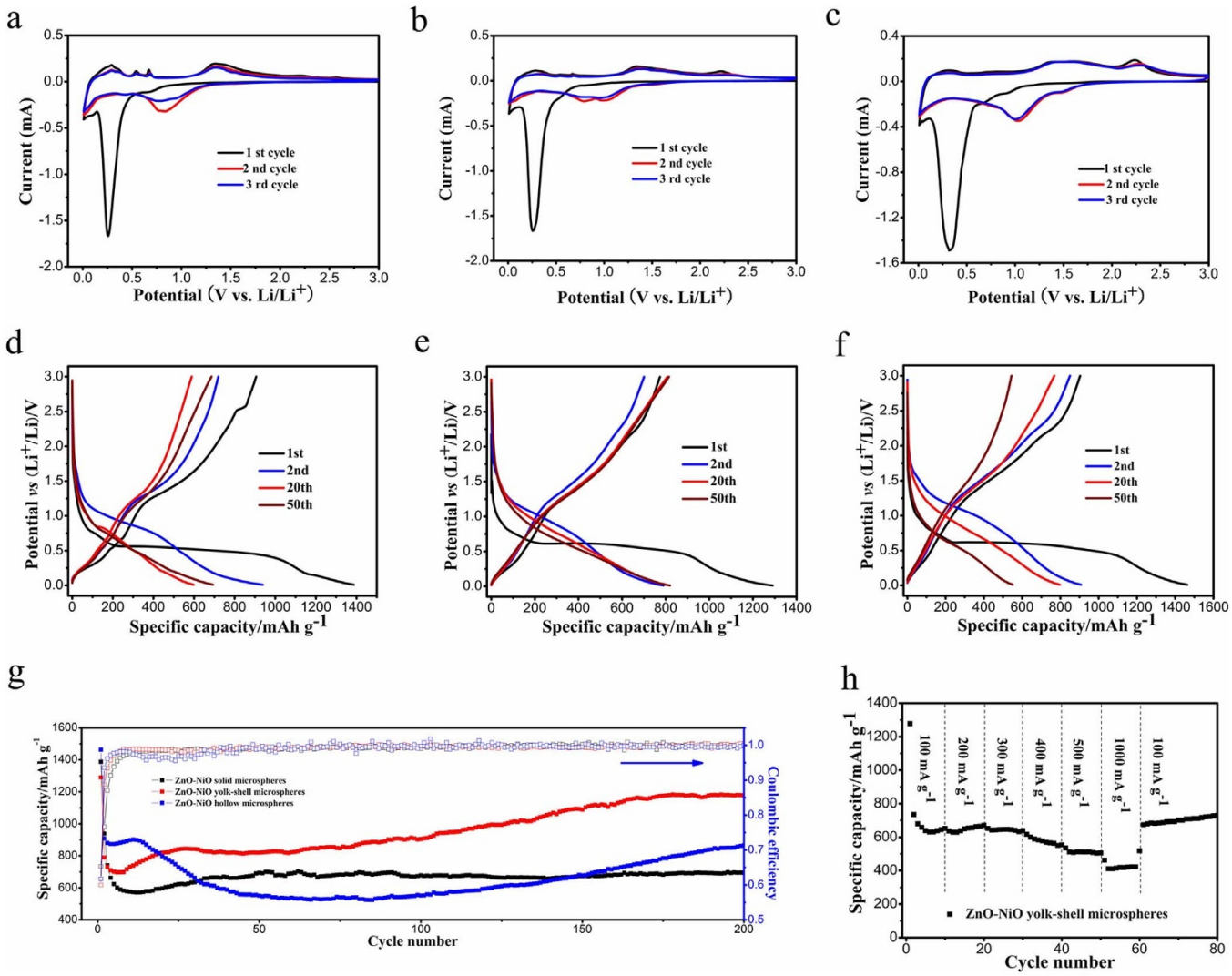

Figure 6 | The first three cyclic voltammogram curves and the galvanostatic discharge-charge profiles ZnO-NiO solid (a,d), yolk-shell (b,e) and hollow (c,f) hybrid microspheres. (g) The discharge capacities and the corresponding Coulombic efficiencies of ZnO-NiO solid, yolk-shell and hollow hybrid microspheres at 100 mA g^{-1}. (h) The rate capabilities of ZnO-NiO yolk-shell hybrid microspheres at different current densities.

with the generation of amorphous Li_2O, the subsequent formation of Zn-Li alloys as well as the solid electrolyte interphase (SEI) films[17,37–40]. In the first anodic scan the oxidation peaks are different in shape and position in three ZnO-NiO anodes. Three peaks nearby 0.29, 0.54 and 0.67 V arose from the multistep dealloying reactions of Zn-Li alloys can be observed obviously for ZnO-NiO solid hybrid microspheres[41]. In the case of ZnO-NiO yolk-shell hybrid microspheres, these three peaks become weaker. For ZnO-NiO hybrid hollow microspheres, a broad and weak peak forms instead of the above three dealloying peaks. The gradually decreasing of ZnO content from solid, yolk-shell to hollow hybrid microspheres may be responsible for the above electrochemical phenomenon[39]. The peaks centered at 1.34 and 2.23 V in the first anodic curves in all three hybrid microspheres electrodes are associated with the regeneration of ZnO and NiO, respectively[20,30,31]. Moreover, the intensity of the peak nearby 2.23 V increases gradually, resulting from the gradually increasing of NiO content from solid, yolk-shell to hollow hybrid microspheres. The CV profiles almost coincide after initial cycle in each electrode, implying the good reversibility of electrode reactions in the subsequent cycles. The electrochemical reactions occurred during lithiation/delithiation process are concluded below:

$$ZnO + 2\,Li^+ + 2\,e^- \leftrightarrow Zn + Li_2O \quad (1)$$

$$NiO + 2\,Li^+ + 2\,e^- \leftrightarrow Ni + Li_2O \quad (2)$$

$$Zn + x\,Li^+ + x\,e^- \leftrightarrow Li_xZn\,(x \le 1) \quad (3)$$

The galvanostatic discharge-charge profiles of ZnO-NiO solid, yolk-shell and hollow hybrid microspheres during the 1st, 2nd, 20th and 50th cycles at 100 mA g^{-1} in 0.01–3.0 V are revealed in Fig. 6d–f. Taking ZnO-NiO yolk-shell hybrid microspheres as an example (Fig. 6e), in the first discharging curve the electrode potential decreases gradually until 0.6 V at which a long and obvious plateau can be seen. This plateau relates to the reduction of ZnO and NiO to Zn and Ni along with the generation of Li_2O[20,30]. Subsequently, a very weak plateau nearby 0.19 V can be discerned carefully, which is caused by the alloying reactions between Zn and Li as well as the formation of SEI layer resulted from the decomposition of electrolyte[20,42]. In the first charge curve, there are three weak plateaus located at 0.31, 1.30 and 2.3 V, which can be attributed to the dealloying reactions of Zn-Li alloys, the oxidation of Zn and Ni to ZnO and NiO, respectively, in good agreement with the above CV results. The discharge-charge curves of ZnO-NiO solid and hollow hybrid microspheres are analogous to that of yolk-shell hybrid microspheres, indicating the similar electrochemical behaviors during cyc-

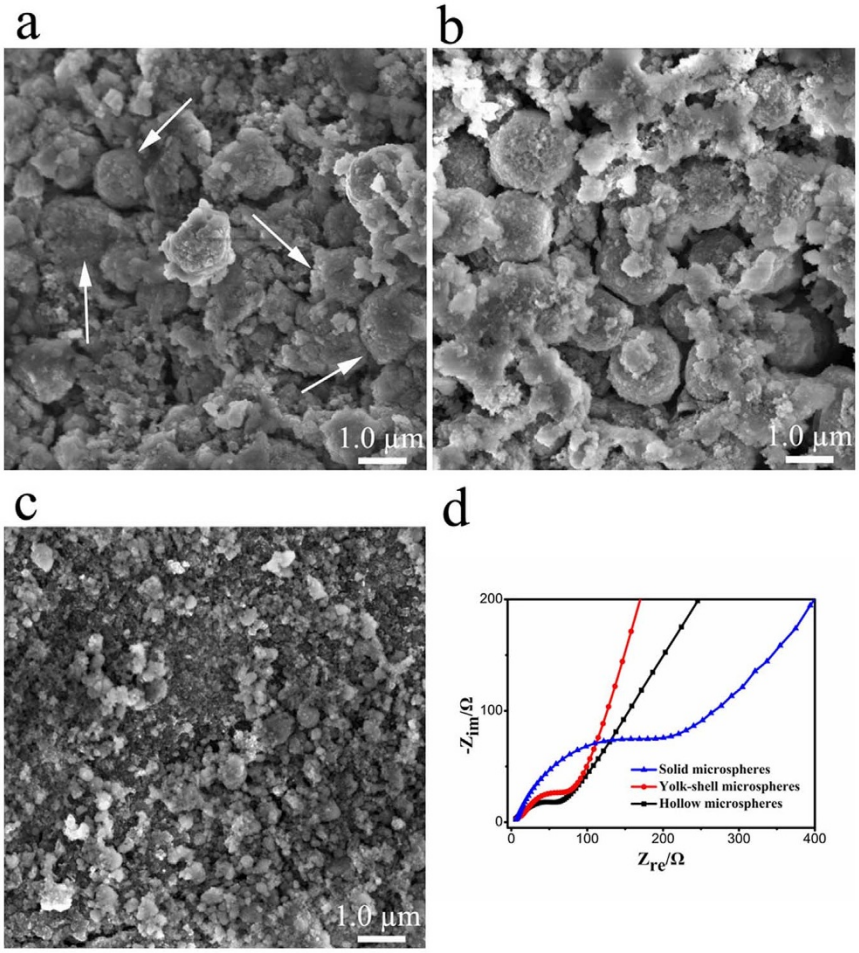

Figure 7 | The SEM images of ZnO-NiO solid (a), yolk-shell (b) and hollow (c) hybrid microspheres after 50th cycles. The white arrows in (a) show some intact ZnO-NiO solid hybrid microspheres. (d) The electrochemical impedance spectra of ZnO-NiO solid, yolk-shell and hollow hybrid microspheres before cycling.

ling. The first discharge/charge capacities of ZnO-NiO solid, yolk-shell and hollow hybrid microspheres are 1387/905, 1290/774 and 1463/903 mA h g^{-1}, respectively. The corresponding irreversible capacity losses during the first cycle are 34.7%, 40.0% and 38.3% for above three electrodes, which are due to the generation of SEI films[20,43].

The discharge capacities and the corresponding Coulombic efficiencies of all three hybrid anodes evaluated at a current density of 100 mA g^{-1} in 0.01–3.0 V are manifested in Fig. 6g. For ZnO-NiO yolk-shell hybrid microspheres, the discharge capacities decrease rapidly in the first 10th cycles and then gradually increase until 170th cycles. From 170th cycle onward, the discharge capacity maintains stably. ZnO-NiO solid hybrid microspheres show the similar trend in discharge capacity to yolk-shell counterparts. The increasing specific capacities can be understood from the following three aspects. First, kinetically activated decomposition of electrolyte, resulting in the reversible formation and dissolution of polymeric gel-like layers on the surface of active materials, can contribute to extra reversible capacity[44–46]. Second, ZnO and NiO nanoparticles contact tightly with each other in the hybrid microspheres. The synergistic effect between ZnO and NiO is good for the improvement of specific capacity[47,48]. Third, the metallic Ni originated from the reduction of NiO can promote the decomposition of Li_2O generated during the lithiation process to some extent, benefitting to increase the specific capacity of electrode materials[49,50]. However, in the case of hollow hybrid microspheres, the discharge capacity slightly increases in the first 12th cycles and then decreases gradually from 13th to 80th cycles. After that, the discharge capacity increases again with cycle number until 200th cycles. The largest surface area of hollow hybrid microspheres (Supplementary Fig. S6) is capable of providing the largest contact area between electrolyte and electrode materials, accounting for the highest specific capacity of hollow hybrid microspheres in the first several cycles. However, the relatively thin shells of ZnO-NiO hollow hybrid microspheres may be not enough to guarantee the electrode integrity due to the drastic volume variation during the repetitive lithium insertion/extraction process, resulting in the pulverization of electrode along with the loss of electronic contact between the active materials and current collectors. As a result, the specific capacity of hollow hybrid microspheres decreases rapidly after 12th cycles. In order to confirm the above hypothesis, all three hybrid anodes after 50th cycles were demolished and the electrode materials were measured by SEM. One can apparently find that almost all of ZnO-NiO yolk-shell hybrid microspheres keep their microspherical morphology after cycling, demonstrating outstanding structural stability (Fig. 7b). Some ZnO-NiO solid hybrid microspheres indicated by arrows can be seen also in Fig. 7a after 50th cycles. However, as shown in Fig. 7c, ZnO-NiO hollow hybrid microspheres obviously crack and disintegrate, well agreeing with the above hypothesis. After 200th cycles, ZnO-NiO solid, yolk-shell and hollow hybrid microspheres deliver the reversible capacities of about 694, 1176 and 865 mA h g^{-1} with the Coulombic efficiencies upon 99%. ZnO-NiO yolk-shell hybrid microspheres possess the highest specific capacity and the best cycling stability than solid and hollow counterparts. For comparison, the

cycling performance of ZnO solid microspheres prepared by calcination of initial zinc citrate solid microspheres at 500°C for 2 h in air is also measured and revealed in Supplementary Fig. S7. The discharge capacity of ZnO solid microspheres decreases quickly to 60 mA h g^{-1} only after 15th cycles, displaying the very poor cycling stability. In addition, the delivered reversible capacity (1176 mA h g^{-1}) of ZnO-NiO yolk-shell hybrid microsphere after 200th cycles is higher than its calculated overall theoretical capacity (887.8 mA h g^{-1}, showed below), revealing the advantages of the combination of ZnO and NiO, and the unique yolk-shell constructing. The rate capability of ZnO-NiO yolk-shell hybrid microspheres are manifested in Fig. 6h. When the current density increases from 100 to 300 mA g^{-1}, the discharge capacity changes no obviously. A high reversible capacity of about 432 mA h g^{-1} can be retained at a large current density of 1000 mA g^{-1}, which is still higher than the theoretical capacity of graphite anode (372 mA h g^{-1}). Impressively, as the current density setting back to 100 mA g^{-1}, the reversible capacity can recover the original values and then gradually increases with cycle number.

The outstanding electrochemical properties of ZnO-NiO yolk-shell hybrid microspheres can be interpreted from the following factors, including the NiO content, specific surface area, microstructure and electronic conductivity. First, the theoretical capacities of ZnO and NiO are 978 and 718 mA h g^{-1}, respectively. The overall theoretical capacities for ZnO-NiO solid, yolk-shell and hollow hybrid microspheres are calculated to be 957.6, 887.8 and 850.3 mA h g^{-1}, respectively, on the basis of the weight percentages of ZnO and NiO in the hybrid microspheres. ZnO-NiO yolk-shell hybrid microspheres with moderate NiO content reveal higher overall theoretical capacity than hollow hybrid counterparts. Second, the larger surface area of ZnO-NiO yolk-shell hybrid microspheres compared to solid hybrid counterparts is capable of providing more electrochemical active sites, which is conducive to enhance the lithium storage properties. Three, the void space in the yolk-shell hybrid microspheres can effectively withstand the mechanical deformation originated from the huge volume change during cycling, which is good for the improvement of cycling stability[35]. On the other hand, previous reports have revealed that yolk-shell micro/nanostructures can accommodate the mechanical deformation more effectively than hollow counterparts during cycling because of the synergistic effect between the cores and shells, and the enhanced mechanical strength[51,52]. Indeed, all of the hollow hybrid microspheres crack after 50th cycles due to their relatively thin shell, while yolk-shell hybrid microspheres basically keep their spherical morphology, displaying good structural stability (Fig. 7). Four, the electrochemical impedance spectra (EIS) of all three hybrid microspheres electrodes before cycling measured at 3 V are illustrated in Fig. 7d. A depressed semicircle in the high-medium frequency region and a straight line in the low frequency region can be seen for each anode. Visibly, the diameter of semicircle increases from hollow, yolk-shell to solid microspheres. This indicates that ZnO-NiO hollow hybrid microspheres possess the smallest charge transfer resistance, followed by yolk-shell and solid microspheres. Accordingly, Ni nanoparticles derived from the reduction of NiO during discharge process possess good electrical conductivity, which is beneficial for the improvement of the overall electrical conductivity of hybrid microspheres electrodes[53,54]. Higher contents of NiO in the hybrid yolk-shell and hollow microspheres would form more Ni nanoparticles during discharge process, accounting for the smaller charge transfer resistances of ZnO-NiO yolk-shell and hollow hybrid microspheres than solid counterparts. Taking all of above factors into account, it can be well understood that ZnO-NiO yolk-shell hybrid microspheres which possess the moderate NiO content, the larger surface area and smaller charge transfer resistance than solid hybrid microspheres, unique yolk-shell configuration as well as more robust structures than hollow hybrid microspheres show the highest specific capacity and the best cyclability.

In summary, zinc-nickel citrate microspheres were successfully fabricated through a facile aging process of zinc citrate solid microspheres in nickel nitrate solution at room temperature. As the concentration of nickel nitrate solution increases, the morphology of the obtained zinc-nickel citrate transform from solid, yolk-shell to hollow microspheres. ZnO-NiO solid, yolk-shell and hollow hybrid microspheres with good morphological inheritance could be prepared by calcination of zinc-nickel citrate solid, yolk-shell and hollow microspheres in air. When applied as the anode materials for lithium ion batteries, ZnO-NiO yolk-shell hybrid microspheres demonstrate the best lithium storage properties than solid and hollow counterparts. The moderate NiO content, larger specific surface area and smaller charge transfer resistance than solid microspheres as well as more robust structures than hollow hybrid microspheres account for the excellent electrochemical properties of yolk-shell hybrid microspheres. These results highlight the significance of elaborate design and rational controlling of the morphology and composition of the electrode materials and simultaneously inspire us to further explore other ZnO-based electrode materials with superior lithium storage properties.

Methods

Synthesis of various zinc-nickel citrate microspheres and ZnO-NiO hybrid microspheres. Zinc citrate solid microspheres were pre-fabricated according to our earlier literature[33]. 0.06 g of zinc citrate solid microspheres were dispersed into 30 ml of 0.15 M nickel nitrate solution and then sonicated to form a uniform suspension. Thereafter, the obtained suspension was aged at room temperature for 1 h to produce zinc-nickel citrate yolk-shell microspheres. To synthesize zinc-nickel citrate solid and hollow microspheres, the concentration of nickel nitrate solution was respectively adjusted to 0.1 and 0.2 M, maintaining other preparation parameters unchanged. To investigate the influence of aging time on the morphology and composition of the obtained zinc-nickel citrate microspheres, the utilized concentration of nickel nitrate solution was 0.1 M and the aging time increased from 1, 2 to 8 h. The collected zinc-nickel citrate solid, yolk-shell and hollow microspheres were calcined at 500°C for 2 h in air to fabricate ZnO-NiO hybrid solid, yolk-shell and hollow microspheres.

Materials characterization. The crystal phases of the acquired zinc-nickel citrate and ZnO-NiO hybrids were characterized on a PANalytical X' pert PRO x-ray diffractometer (Cu Kα radiation 40 kV, 30 mA). Scanning electron microscopy (Hitachi SU-70) and transmission electron microscopy (JEM-2100, 200 kV) were used to disclose the morphology and microstructure of the samples. Fourier-transform infrared (FTIR) spectrum and thermogravimetric (TG) evaluation were respectively conducted on Nicolet Nexus-670 FT-IR spectrometer and SDT-Q600 thermal analyzer. The specific surface area and pore diameter distributions were recorded on a TriStar 3020 system.

Electrochemical evaluations. The coin 2025 cells were assembled in an argon-filled glove box adopting metal lithium tablets and 1 M $LiPF_6$ in ethylene carbonate and diethyl carbonate (1 : 1, v/v) as the counter electrode and electrolyte, respectively. 70 wt% of active materials (ZnO-NiO hybrid microspheres), 20 wt% of acetylene black and 10 wt% of poly (vinyl difluoride) (PVDF) were uniformly mixed in 1-methyl-2-pyrrolidinone (NMP) under vigorously magnetic stirring. The formed slurry was pasted on a copper foil substrate, kept at 80°C for 12 h and then pressed to fabricate the working electrode. The separator is polypropylene film (Celgard 2400). Neware multiple battery testers were applied to measure the galvanostatic discharge/charge capacities of the electrodes. Autolab electrochemical workstation (NOVA 1.9) was employed for the characterizations of Cyclic voltammetry and electrochemical impedance spectra.

1. Han, J. T., Huang, Y. H. & Goodenough, J. B. New anode framework for rechargeable lithium batteries. *Chem. Mater* **23**, 2027–2029 (2011).
2. Guo, H. *et al*. Morphology-controlled synthesis of SnO_2/C hollow core-shell nanoparticle aggregates with improved lithium storage. *J. Mater. Chem. A* **1**, 3652–3658 (2013).
3. Reddy, M. V., Subba Rao, G. V. & Chowdari, B. V. R. Metal oxides and oxysalts as anode materials for Li ion batteries. *Chem. Rev.* **113**, 5364–5457 (2013).
4. Yuan, C., Wu, H. B., Xie, Y. & Lou, X. W. Mixed transition-metal oxides: design, synthesis, and energy-related applications. *Angew. Chem. Int. Ed.* **53**, 1488–1504 (2014).
5. Bruce, P. G., Scrosati, B. & Tarascon, J. M. Nanomaterials for rechargeable lithium batteries. *Angew. Chem. Int. Ed.* **47**, 2930–2946 (2008).
6. Hu, M. *et al*. Synthesis of superparamagnetic nanoporous iron oxide particles with hollow interiors by using prussian blue coordination polymers. *Chem. Mater* **24**, 2698–2707 (2012).

7. Weng, W. *et al.* A High-speed passive-matrix electrochromic display using a mesoporous TiO_2 electrode with vertical porosity. *Angew. Chem. Int. Ed.* **49**, 3956–3959 (2010).
8. Oveisi, H. *et al.* Unusual antibacterial property of mesoporous titania films: drastic improvement by controlling surface area and crystallinity. *Chem. Asian J.* **5**, 1978–1983 (2010).
9. Xu, S. *et al.* α-Fe_2O_3 multi-shelled hollow microspheres for lithium ion battery anodes with superior capacity and charge retention. *Energy Environ. Sci.* **7**, 632–637 (2014).
10. Zhang, C., Chen, Z., Guo, Z. & Lou, X. W. Additive-free synthesis of 3D porous V_2O_5 hierarchical microspheres with enhanced lithium storage properties. *Energy Environ. Sci.* **6**, 974–978 (2013).
11. Zhuo, L. *et al.* Facile synthesis of a Co_3O_4-carbon nanotube composite and its superior performance as an anode material for Li-ion batteries. *J. Mater. Chem. A* **1**, 1141–1147 (2013).
12. He, M. *et al.* A SnO_2@carbon nanocluster anode material with superior cyclability and rate capability for lithium-ion batteries. *Nanoscale* **5**, 3298–3305 (2013).
13. Lee, S. M., Choi, S. H., Lee, J. K. & Kang, Y. C. Electrochemical properties of graphene-MnO composite and hollow-structured MnO powders prepared by a simple one-pot spray pyrolysis process. *Electrochim. Acta* **132**, 441–447 (2014).
14. Sun, Z. *et al.* Generalized self-assembly of scalable two-dimensional transition metal oxide nanosheets. *Nature Commun* **5**, 3813–3821 (2014).
15. Sun, Z. *et al.* Robust superhydrophobicity of hierarchical ZnO hollow microspheres fabricated by two-step self-assembly. *Nano Research* **6**, 726–735 (2013).
16. Sun, Z. *et al.* Architecture designed ZnO hollow microspheres with wide-range visible-light photoresponses. *J. Mater. Chem. C.* **1**, 6924–6929 (2013).
17. Huang, X., Xia, X., Yuan, Y. & Zhou, F. Porous ZnO nanosheets grown on copper substrates as anodes for lithium ion batteries. *Electrochim. Acta* **56**, 4960–4965 (2011).
18. Usui, H., Kono, T. & Sakaguchi, H. Novel composite thick-film electrodes consisted of zinc oxide and silicon for lithium-ion battery anode. *Int. J. Electrochem. Sci.* **7**, 4322–4334 (2012).
19. Wang, Z., Zhou, L. & Lou, X. W. Metal oxide hollow nanostructures for lithium-ion batteries. *Adv. Mater.* **24**, 1903–1911 (2012).
20. Xie, Q. *et al.* Yolk-shell ZnO-C microspheres with enhanced electrochemical performance as anode material for lithium ion batteries. *Electrochim. Acta* **125**, 659–665 (2014).
21. Son, M. Y., Hong, Y. J. & Kang, Y. C. Superior electrochemical properties of Co_3O_4 yolk-shell powders with a filled core and multishells prepared by a one-pot spray pyrolysis. *Chem. Commun* **49**, 5678–5680 (2013).
22. Choi, S. H. & Kang, Y. C. Ultrafast synthesis of yolk-shell and cubic NiO nanopowders and application in lithium ion batteries. *ACS Appl. Mater. Interfaces* **6**, 2312–2316 (2014).
23. Wang, B., Wu, H. B., Zhang, L. & Lou, X. W. Self-supported construction of uniform Fe_3O_4 hollow microspheres from nanoplate building blocks. *Angew. Chem. Int. Ed.* **52**, 4165–4168 (2013).
24. Wang, X. *et al.* Synthesis and lithium storage properties of Co_3O_4 nanosheet-assembled multishelled hollow spheres. *Adv. Funct. Mater* **20**, 1680–1686 (2010).
25. Zhang, G. & Lou, X. W. General synthesis of multi-shelled mixed metal oxide hollow spheres with superior lithium storage properties. *Angew. Chem* **126**, 9187–9190 (2014).
26. Li, Z., Li, B., Yin, L. & Qi, Y. Prussion blue-supported annealing chemical reaction route synthesized double-shelled Fe_2O_3/Co_3O_4 hollow microcubes as anode materials for lithium-ion battery. *ACS Appl. Mater. Interfaces* **6**, 8098–8107 (2014).
27. Choi, S. H. & Kang, Y. C. Using simple spray pyrolysis to prepare yolk-shell-structured ZnO-Mn_3O_4 systems with the optimum composition for superior electrochemical properties. *Chem. Eur. J.* **20**, 3014–3018 (2014).
28. Yang, K. M., Hong, Y. J. & Kang, Y. C. Electrochemical properties of yolk-shell-structured CuO-Fe_2O_3 powders with various Cu/Fe molar ratios prepared by one-pot spray pyrolysis. *ChemSusChem* **6**, 2299–2303 (2013).
29. Chen, J. S. *et al.* One-pot formation of SnO_2 hollow nanospheres and α-Fe_2O_3@SnO_2 nanorattles with large void space and their lithium storage properties. *Nanoscale* **1**, 280–285 (2009).
30. Ju, Z., Guo, C., Qian, Y., Tang, B. & Xiong, S. Direct large-scale synthesis of 3D hierarchical mesoporous NiO microspheres as high-performance anode materials for lithium ion batteries. *Nanoscale* **6**, 3268–3273 (2014).
31. Sasidharan, M., Gunawardhana, N., Senthil, C. & Yoshio, M. Micelle templated NiO hollow nanospheres as anode materials in lithium ion batteries. *J. Mater. Chem. A* **2**, 7337–7344 (2014).
32. Zhou, G., Ma, J. & Chen, L. Selective carbon coating techniques for improving electrochemical properties of NiO nanosheets. *Electrochim. Acta* **133**, 93–99 (2014).
33. Xie, Q., Li, J., Tian, Q. & Shi, R. Template-free synthesis of zinc citrate yolk-shell microspheres and their transformation to ZnO yolk-shell nanospheres. *J. Mater. Chem.* **22**, 13541–13547 (2012).
34. Cho, S. *et al.* Formation of amorphous zinc citrate spheres and their conversion to crystalline ZnO nanostructures. *Langmuir* **27**, 371–378 (2010).
35. Vu, A., Qian, Y. & Stein, A. Porous electrode materials for lithium-ion batteries-how to prepare them and what makes them special. *Adv. Energy Mater.* **2**, 1056–1085 (2012).
36. Zhao, Y. & Jiang, L. Hollow micro/nanomaterials with multilevel interior structures. *Adv. Mater.* **21**, 3621–3638 (2009).
37. Gao, X. P. & Yang, H. X. Multi-electron reaction materials for high energy density batteries. *Energy Environ. Sci.* **3**, 174–189 (2010).
38. Zhang, G. *et al.* Synthesis of mesoporous NiO nanospheres as anode materials for lithium ion batteries. *Electrochim. Acta* **80**, 140–147 (2012).
39. Qiao, L. *et al.* Single electrospun porous NiO-ZnO hybrid nanofibers as anode materials for advanced lithium-ion batteries. *Nanoscale* **5**, 3037–3042 (2013).
40. Shen, X., Mu, D., Chen, S., Wu, B. & Wu, F. Enhanced electrochemical performance of ZnO-loaded/porous carbon composite as anode materials for lithium ion batteries. *ACS Appl. Mater. Interfaces* **5**, 3118–3125 (2013).
41. Wang, H., Pan, Q., Cheng, Y., Zhao, J. & Yin, G. Evaluation of ZnO nanorod arrays with dandelion-like morphology as negative electrodes for lithium-ion batteries. *Electrochim. Acta* **54**, 2851–2855 (2009).
42. Pan, Q., Qin, L., Liu, J. & Wang, H. Flower-like ZnO-NiO-C films with high reversible capacity and rate capability for lithium-ion batteries. *Electrochim. Acta* **55**, 5780–5785 (2010).
43. Liu, L. *et al.* Hollow NiO nanotubes synthesized by bio-templates as the high performance anode materials of lithium-ion batteries. *Electrochim. Acta* **114**, 42–47 (2013).
44. Wang, X. *et al.* Mesoporous NiO nanosheet networks as high performance anodes for Li ion batteries. *J. Mater. Chem. A* **1**, 4173–4176 (2013).
45. Wei, W. *et al.* 3D Graphene foams cross-linked with pre-encapsulated Fe_3O_4 nanospheres for enhanced lithium storage. *Adv. Mater.* **25**, 2909–2914 (2013).
46. Li, L., Seng, K. H., Chen, Z., Guo, Z. & Liu, H. K. Self-assembly of hierarchical star-like Co_3O_4 micro/nanostructures and their application in lithium ion batteries. *Nanoscale* **5**, 1922–1928 (2013).
47. Feng, Y., Zou, R., Xia, D., Liu, L. & Wang, X. Tailoring CoO-ZnO nanorod and nanotube arrays for Li-ion battery anode materials. *J. Mater. Chem. A* **1**, 9654–9658 (2013).
48. Sun, Z. *et al.* Facile fabrication of hierarchical $ZnCo_2O_4$/NiO core/shell nanowire arrays with improved lithium-ion battery performance. *Nanoscale* **6**, 6563–6568 (2014).
49. Li, X., Dhanabalan, A. & Wang, C. Enhanced electrochemical performance of porous NiO-Ni nanocomposite anode for lithium ion batteries. *J. Power Sources* **196**, 9625–9630 (2011).
50. Huang, X. *et al.* Electrochemical properties of NiO-Ni nanocomposite as anode material for lithium ion batteries. *J. Power Sources* **161**, 541–544 (2006).
51. Li, W. Y., Xu, L. N. & Chen, J. Co_3O_4 nanomaterials in lithium-ion batteries and gas sensors. *Adv. Funct. Mater* **15**, 851–857 (2005).
52. Ding, Y. L. *et al.* Double-shelled hollow microspheres of $LiMn_2O_4$ for high-performance lithium ion batteries. *J. Mater. Chem.* **21**, 9475–9479 (2011).
53. Su, L., Zhou, Z. & Shen, P. Ni/C hierarchical nanostructures with Ni nanoparticles highly dispersed in N-containing carbon nanosheets: origin of Li storage capacity. *J. Phys. Chem. C* **116**, 23974–23980 (2012).
54. Mai, Y. J. *et al.* Self-supported nickel-coated NiO arrays for lithium-ion batteries with enhanced capacity and rate capability. *Electrochim. Acta* **67**, 73–78 (2012).

Acknowledgments

The authors gratefully acknowledge financial support from the National Basic Research Program of China (No. 2012CB933103), the National Outstanding Youth Science Foundation of China (Grant No. 50825101), the National Natural Science Foundation of China (Grant Nos. 51171158 and 51371154) and the Fundamental Research Funds for the Central Universities of China (Grant no. 201312G003).

Author contributions

Q.X. and D.P. designed experiments, analyzed data and co-wrote the paper. Q.X., Y.T. and D.Z. carried out the experiments. L.S. and G.Y. contributed to discussions. All authors reviewed the manuscript.

Additional information

Supplementary information accompanies this paper at http://www.nature.com/scientificreports

Competing financial interests: The authors declare no competing financial interests.

How to cite this article: Xie, Q. *et al.* Facile fabrication of various zinc-nickel citrate microspheres and their transformation to ZnO-NiO hybrid microspheres with excellent lithium storage properties. *Sci. Rep.* **5**, 8351; DOI:10.1038/srep08351 (2015).